Advances in Science and Technology Research Journal

Advances in Science and Technology Research Journal, 2025, 19(11), 414–428
https://doi.org/10.12913/22998624/209177
ISSN 2299-8624, License CC-BY 4.0

Received: 2025.07.02
Accepted: 2025.09.15
Published: 2025.10.01

Effect of surface charge and gap distance on electroadhesive forces in electret films

Tomasz Czapka[1], Adam Pelesz[1*]

[1] Department of Electrical Engineering Fundamentals, Wroclaw University of Science and Technology, Wyb. St. Wyspianskiego 27, 50-370, Wroclaw, Poland
* Corresponding author's e-mail: adam.pelesz@pwr.edu.pl

ABSTRACT

Electroadhesion (EA) is the phenomenon of surface adhesion caused by electrostatic attraction due to electric fields, whether externally applied or originating from quasi-permanent surface charges (i.e., passive EA). In the presented study, the adhesion force was provided by the charges stored in the electret polyethylene terephthalate (PET) film. This study provides a clear and quantitative understanding of how a PET electret film behaves as a passive electroadhesive material. The tested film was charged via direct-current corona discharge (point-plane electrode configuration, ±10 kV) to impart a quasi-permanent surface charge. Key charge-storage characteristics (including surface potential distribution and charge decay time) were measured. This characterisation revealed a non-uniform (bell-shaped) surface potential profile and long charge storage time on the PET film ($t_{95\%} > 980$ s). Next, the electrostatic adhesion force between the charged film and a grounded conductive surface was quantified at various film-surface separations (0.5 mm to tens of millimeters) using a precision force measurement setup. The attractive force increases with the film surface charge and decreases steeply with increasing separation distance, reaching approximately 16.6 mN at a 0.5 mm separation (corresponding to a surface charge density of about 4.2 mC/m²). These results demonstrate the feasibility of corona-charged PET as a low-power electroadhesive material.

Keywords: DC corona discharge, dielectric film, electroadhesion, electret, polyethylene terephthalate (PET).

INTRODUCTION

Electrostatic forces and coulomb's law

Electrostatic forces are a pivotal aspect of physics and materials science, playing a crucial role across numerous applications, especially in the fields of biomedicine, materials engineering, and environmental science. Understanding electrostatic interactions is essential for grasping the mechanisms underlying various physical and chemical processes.

Electrostatic forces, also referred to as Coulombic forces, arise from the interaction between charged particles. They can be categorised mainly into attraction and repulsive forces, which are governed by Coulomb's law [1–3]. This law states that the magnitude of the electrostatic force between two point charges is directly proportional to the product of the magnitudes of the charges and inversely proportional to the square of the distance between them [1]. Attractive forces occur between opposite charges, while like charges (i.e., charges of the same polarity) experience a repulsive force, affecting particle behaviour in solutions and materials. Consequently, Coulomb's law in vacuum takes the following form:

$$F_e = \frac{1}{4\pi\varepsilon_0}\frac{q_1 \cdot q_2}{r^2} \tag{1}$$

where: F_e is the magnitude of the electrostatic force between the charges q_1 and q_2, ε_o is the permittivity of free space, and r refers to the distance between two charges.

The principle of superposition states that the total force F_{Te} acting on a given charge in the presence of multiple other charges is the vector sum of the individual forces $F_{e\cdot i}$ exerted by each of those charges [1–3]:

$$\vec{F}_{Te} = \sum_i \vec{F}_{e\text{-}i} \tag{2}$$

It is important to emphasise that Coulomb's law, as expressed in Equation 1, is strictly valid only for point charges or spherically symmetric charge distributions. In the cases involving more complex geometries, the force must be determined by evaluating the electric field generated by continuous charge distributions.

For example, in the case of an ideal parallel-plate capacitor, where the plates have a large surface area s and are positioned close to each other, the resulting force does not obey the inverse-square law. Instead, assuming a uniform electric field and a constant charge Q_0 on the plates, the attractive force between them becomes independent of the plate separation (i.e., spacing between electrodes) d and is given by [3]:

$$F_{Ce} = \frac{1}{2} \cdot \frac{Q_0^2}{\varepsilon_0 \cdot s} \tag{3}$$

In many complex systems, an exact analytical expression for the electrostatic force is often difficult to establish due to geometric complexity, the presence of pronounced edge effects (i.e., fringing effects in real capacitors), and the non-uniform distribution of material properties. Spatial inhomogeneities in dielectric permittivity—arising from multilayer structures, material gradients, or interfacial regions between charged bodies—can also substantially alter the electric field distribution and, consequently, the resulting force F. In such cases, experimental validation becomes essential, particularly for configurations designed for practical applications.

Electrostatic forces play a fundamental role in understanding phenomena such as static electricity, the behaviour of particles in electric fields, and the operation of devices including capacitors and electrostatic precipitators [1]. Numerous industrial and technological applications also exploit electrostatic effects, including inkjet printers, photocopiers, electrostatic motors, separators, ion propulsion systems, and microelectromechanical systems (MEMS) [1, 2, 4].

In modern technology, electrostatic forces find applications in numerous domains. In nanotechnology, for instance, electrostatic interactions enable the fabrication of nanomaterials through techniques such as colloidal dispersions and nanocrystal assembly, where the precise control of charges and surface potentials allows for the manipulation of material properties at the molecular level [5]. Furthermore, electrostatic forces are crucial in such methods as inkjet printing for biological applications, where precise alignments of biomolecules are achieved by modulating electrostatic interactions [5].

Another prominent application of electrostatics is microelectromechanical systems (MEMS). These devices rely on electrostatic actuation, where varying voltage differences create forces that lead to mechanical movement. The quick response times and high accuracy of electrostatic actuators make them ideal for various applications, including sensors and communication technologies [6] as well as force microscopy devices that enable the imaging of material properties at the atomic scale [7]. Additionally, electrostatic forces play an important role in energy harvesting systems, such as triboelectric nanogenerators, which convert mechanical energy into electrical energy using contact charging (i.e., electrification) principles [8].

In biomedicine, electrostatic interactions are fundamental for the design of drug delivery systems. The targeted binding of drugs to specific cell types can be manipulated through charge interactions, ensuring that therapeutic agents are delivered where needed, enhancing treatment efficacy while minimising side effects [9]. Furthermore, electrostatic forces facilitate the encapsulation of biomolecules within carriers, leveraging charge interactions to form stable complex structures [10].

Electrostatic adhesion

Electroadhesion (EA) refers to the electrostatic attraction between two surfaces when an electric field is present between them. This electric field may originate from an external power source and be actively switched on and off (i.e., active EA), or it may result from a quasi-permanent surface charge, in which case the field is continuously present (i.e., passive EA). EA systems offer unique advantages, including the ability to grip a wide range of materials (metals, glass, concrete, fabrics, etc.) with minimal surface damage and very low energy consumption compared to suction or magnetic methods [11, 12]. However, conventional, active electroadhesion requires a continuous high-voltage supply to maintain the adhesive force, which can introduce complexity and some limitations. Recent developments have expanded electroadhesion beyond the traditional, active mode (i.e., with an external voltage source) into passive modes that rely on stored electrostatic

charge (i.e., using electret materials or temporary charging) without continuous power.

Active electroadhesion employs an external high-voltage power supply and electrode arrangements to dynamically create and control electrostatic attraction. In this mode, a controller can switch the voltage on or off (or even modulate it), thereby engaging or releasing the adhesive force almost instantly. Some applications utilising active electroadhesion include object fixturing [13], robotic crawling and climbing [14, 15], mechanical and electrical interconnections [16], perching [17], anchoring [18], as well as robotic grippers [19].

Generally, an electroadhesive system consists of four key elements: an EA electrode, a high-voltage power supply, a control module, and a substrate material to be attached or lifted [20]. Active electroadhesion devices typically operate at voltages of up to a few tens of kilovolts, but with extremely low currents (microampere-range), meaning their power consumption is very low despite the high voltage [11, 12]. A drive circuit applies either DC or AC high voltage. Many systems use a DC bias with alternating-polarity electrodes to avoid net charging of the surface (which could attract dust or cause sticking after power-off). When activated, the pad will adhere to almost any material: metal, wood, glass, plastic, paper, fabric, and even rough or dusty surfaces [11]. This broad compatibility arises because the electric field either induces image charges in conductors or polarises the molecules of insulators. In contrast to suction cups or magnets, electroadhesion does not require an airtight seal or ferromagnetic material – it works on porous and non-magnetic materials as well.

On the other hand, passive electroadhesion techniques do not require continuous power input. In passive EA, the adhesive force is provided by the charges stored in the materials themselves (i.e., using charged dielectric layers – electret materials), eliminating the need for an active voltage source during operation [21, 22]

Electret materials enable such passive electroadhesion. An electret is a dielectric material that carries a quasi-permanent electric charge or dipole polarisation, analogous to a permanent magnet but with an electric field. Once charged (e.g., by a corona discharge or other charging method), an electret can induce opposite charges on a nearby surface, creating an adhesive electrostatic force without any external power supply. Passive electroadhesive devices based on electrets can therefore be extremely thin, flexible, and energy-efficient. They remain "on" with zero power consumption, offering possibilities for applications in robotics, manufacturing, and consumer products. For instance, a recent study demonstrated electret-based electroadhesion for enhancing friction, underscoring the potential of passive EA in robotic gripping and locomotion systems [23].

Despite this promise, several challenges and knowledge gaps remain for electret-based electroadhesion. All electrets gradually lose their charge over time, especially under adverse conditions like high humidity or surface contamination, which can significantly reduce long-term adhesion performance [22]. Moreover, the maximum achievable adhesive force in a passive system is fundamentally limited by the surface charge density that the electret material can hold. These practical limitations mean that the durability and strength of passive EA devices depend critically on the charge storage and retention characteristics of an electret (also known as lifetime characteristics or charge decay characteristics).

The examples above demonstrate the versatility of electroadhesion as a functional mechanism in fields ranging from robotics and electronics to consumer goods and healthcare. Further development of materials and optimisation of electrode configurations—or electret charging methods such as corona discharge—are expected to further expand the application of the so-called passive electroadhesion process.

Motivation and aim of this work

The aim of this study was twofold:

- to investigate the influence of various DC corona charging conditions (varying the charging voltage magnitude and polarity) on the total charge and surface potential distribution on the PET to evaluate the charge decay rate, thereby determining how long the film can retain its charged (electret) state;
- to estimate the electrostatic adhesion forces between the charged PET film and a grounded conductive surface at various film–surface separation distances.

The scientific objectives of this work result from the lack of comprehensive academic research into the fundamental aspects related to passive electroadhesion. Although some commercial products (e.g., reusable glue-free posters and removable

labels) already utilise static charge to adhere to surfaces, detailed studies of their charge decay behaviour and electroadhesive mechanism under real-world conditions remain limited. This lack of fundamental data in the literature hinders the optimisation and wider adoption of passive electroadhesion technology in advanced applications, since designers have little quantitative guidance on how long a polymer electret can hold its charge or how much force it can reliably provide over time. To bridge this gap, this study investigated the novel use of polyethylene terephthalate (PET) film as an electret material for passive electroadhesion.

Nowadays, PET is a widely used polymer with high electrical resistivity and good mechanical stability, making it a suitable material for electret-based adhesion. Furthermore, PET can be applied in many new applications in various technologies, e.g., 3D printing, the development of energy-absorbing structures, or as an additive to concrete to improve its mechanical properties and durability [24–26].

MATERIALS AND METHODS

Electret films

A commercially available PET film was used as the electret material. The tested film was purchased from Mitsubishi Polyester Film GmbH (Germany). The volume resistivity (r_v) and relative permittivity (ε_r) of the polymeric film were equal to 10^{15} Ω·m (measured) and 3.26 (data supported by the manufacturer, not measured), respectively. Each sample was a circular PET sheet 70 mm in diameter and 36 μm thick.

Corona charging of polymeric films

Corona charging was conducted in ambient air at atmospheric pressure. A single-needle high-voltage corona electrode (connected to a Glassman high-voltage DC power supply) was used to charge the film. The applied corona voltage U_e was varied from –10 kV to +10 kV. The needle tip was positioned 15 mm above the sample surface, and each film was exposed to the corona discharge for 30 s. The corona discharge process proceeded under fixed conditions of temperature and humidity, i.e., for $T = 22 \pm 1$ °C and $RH = 40 \pm 2\%$. During charging, the side of the PET film opposite the needle was held in contact with a grounded metal plate (Figure 1). For clarity, the surface of the sample facing the corona electrode is referred to as "side A" (charged side), and the opposite surface that was against the grounded plate is referred to as "side B" (grounded side).

Measurement of charge decay time and charge level

Immediately after corona charging, the surface potential of each film was measured using a Trek Model 341B electrostatic voltmeter with a non-contacting probe. For this measurement, the charged film was placed on a grounded conductive plate, and the probe was held at a distance of 2 mm above the film surface (Figure 2). The probe was then scanned across the sample in the x–y plane to map the surface potential distribution over the film. In addition to the surface potential mapping, the total charge on the film was measured using a Faraday cup connected to an RFT-6305 analog electrometer. This net charge measurement was used to correlate with the surface potential

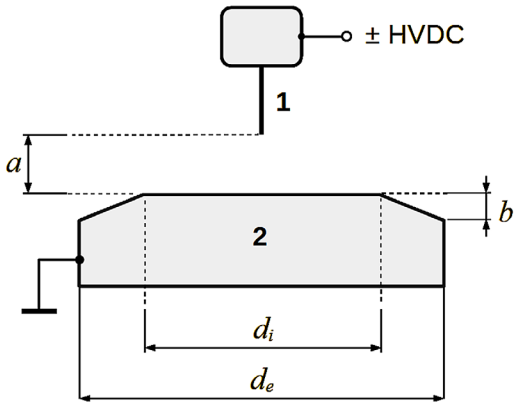

Figure 1. Schematic of the corona charging setup (not to scale): (1) high-voltage needle electrode, (2) grounded plate electrode, a – adjustable gap, d_i = 45 mm, d_e = 70 mm, b = 5 mm (geometric parameters)

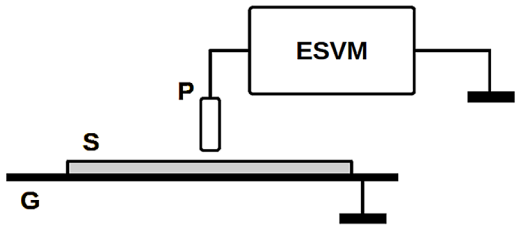

Figure 2. Experimental setup for surface potential decay measurements: G – grounded plate, S – sample, P – measuring probe, ESVM – electrostatic voltmeter

map of the electret sample.The measurements were carried out under fixed conditions of temperature and humidity, i.e., for T = 22 ± 1 °C and RH = 40 ± 2%.

Electrostatic force measurements

After charging, the electrostatic attraction force between the charged film and a grounded conductive surface was measured using a sensitive weighing method. The charged PET film was clamped between two concentric brass rings that were connected to ground (Figure 3). The inner brass ring had a diameter of 44 mm, and the outer ring had a diameter of 51 mm (with a small gap in between, as shown in Figure 3). This ring-supported film assembly was then positioned at a set distance above the metal weighing pan of a digital balance with an accuracy of 0.001 g (OHAUS Corporation, USA) as presented in Figure 4. A vertical translation stage (z-axis) allowed precise adjustment of the gap between the film and the balance platform, with a positioning accuracy of 0.1 mm. During each force measurement, the brass ring fixture (holding the film) and the metal plate of the balance were both grounded to ensure a common reference potential for the system. All measurements were performed under fixed conditions of temperature and humidity, i.e., for T = 22 ± 1 °C and RH = 40 ± 2%.

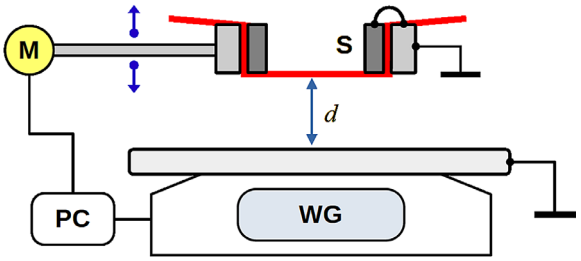

Figure 4. Schematic diagram of the electrostatic force measurement system: S – sample (PET film), M – positioning control unit, WG – weighing scale (digital balance), PC – data acquisition system

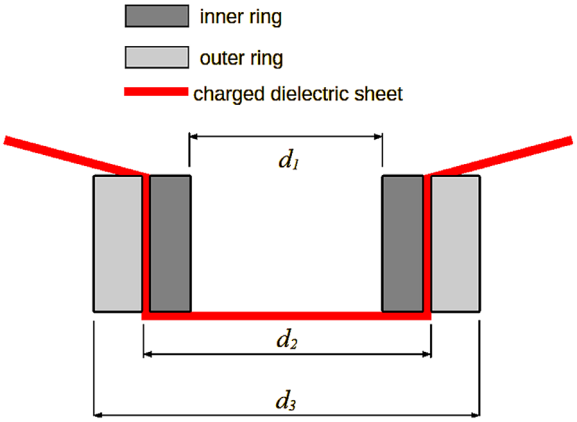

Figure 3. Method of mounting the PET film between grounded brass rings (ring diameters: d_1 = 44 mm, d_2 = 47 mm, d_3 = 51 mm)

RESULTS AND DISCUSSION

Potential decay

To evaluate the charge retention of the PET film and confirm its electret behaviour, the surface potential decay was measured on both the directly charged side (side A, facing the corona electrode) and the opposite side (side B, in contact with the grounded plate during charging). Representative decay curves (Figure 5) show that negatively charged samples lose surface potential more rapidly than positively charged ones.

Table 1 provides the initial surface potentials (U_i) and the time required for the potential to drop to 95% of its initial value ($t_{95\%}$) for each case. The obtained experimental data indicate a much

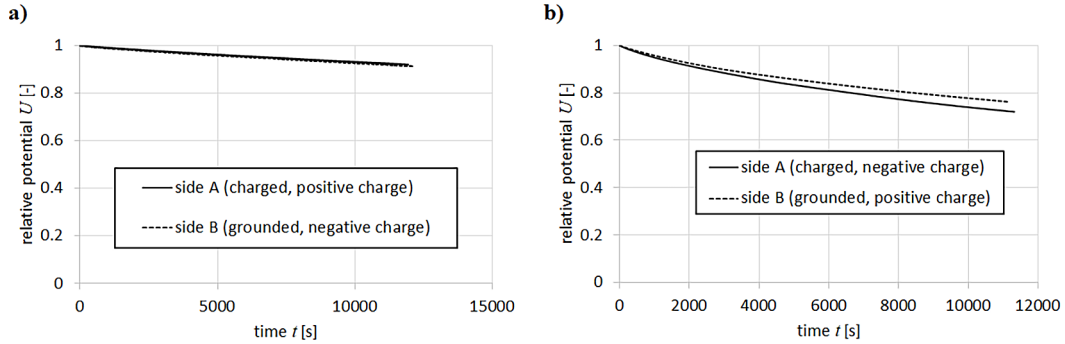

Figure 5. Electric potential decay for: a) positively, and b) negatively charged samples. The results were obtained for voltage U_e and charging time t_e equal to ± 10 kV and 30 s, respectively

Table 1. Average charge decay times for the studied cases

Case	U_i [kV]	$t_{95\%}$ [s]
U_e = +10 kV (charged side, positive charge)	4.82	6900
U_e = +10 kV (grounded side, negative charge)	-4.87	6300
U_e = -10 kV (charged side, negative charge)	-5.21	980
U_e = -10 kV (grounded side, positive charge)	5.11	1200

slower decay of surface potential for positively charged PET film than for negatively charged samples. In practical terms, a PET electret charged with a voltage of +10 kV retains charge for hours (with $t_{95\%}$ around 1.75–1.9 hours), whereas a negatively charged PET sample retains charge within tens of minutes. This asymmetry suggests that the underlying charge trapping and leakage processes are highly sensitive to the charge polarity, i.e., polarity of the corona electrode. The polarity-dependent behaviour observed in PET is part of a broader pattern reported for various electret materials. For instance, Molinié [27] noted that on moderate fields, electrets like PTFE and FEP show markedly different stability for positive vs. negative corona charging (especially after thermal trap stabilization by annealing). Rychkov et al. reported that untreated FEP films lose positive charge much faster than negative charge, but after a chemical surface treatment, the positive charge stability increased by about two orders of magnitude, effectively eliminating the inherent asymmetry [28]. These findings demonstrate that charge-decay asymmetry is rooted in material properties (surface and bulk trap characteristics), and that modifying the surface of a material can preferentially enhance the stability of one charge polarity over the other. Additionally, surface potential decay in polymers (including PET) is influenced by environmental factors (e.g., temperature and humidity) and by initial charge density (the so-called "cross-over effect") [27, 29]. In the case of PET charged via corona discharge, the charging polarity plays a decisive role in how charges are deposited and subsequently retained on the film.

Slight differences in surface potential decay (SPD) behaviour between the two sides of the sample were observed. For example, in the case of a negative charging voltage, SPDs to 95% of the initial value for both sample sides are equal to 980 and 1200 s, respectively. A similar effect is also observed when the corona electrode is supplied with a voltage of positive polarity. However, the observed differences in SPD are also related to the initial charge level of the samples. As it can be seen, higher surface potential values lead to a reduction in SPD. SPDs for samples with initial surface potentials of 4.82 and 4.87 kV, for example, are 6900 and 6300 s, respectively. Despite these side-to-side differences, it is evident that the PET film retains its charge for sufficiently long durations to perform the electroadhesion force measurements.

Beyond the obtained results, prior studies have shown that the corona charging process can improve charge storage in various polymers. For instance, Zhang et al. demonstrated that corona charging can enhance the charge density and stability of polypropylene electrets by modifying local charge centers and trap distributions [30, 31]. Similarly, Hu et al. proved that the charging process contributes to deeper electron traps in polymer constructs, thereby stabilising stored charges [32]. This improvement is critical in applications such as filtration, where the performance of electret-based materials is directly correlated with their charge storage abilities [33]. In general, electret charge can be stored either as real (embedded) charges or as oriented dipoles, and the dominant mechanism depends on the material. For example, non-fluoropolymer electrets often rely on dipolar polarisation, whereas corona-injected space charges are particularly effective for fluorinated polymers due to their superior charge lifetime [32]. For example, Dai et al. observed that corona-charged FEP films exhibit very stable surface potentials for both polarities (long lifetimes for negative and positive charges) [34]. Moreover, changes in material processing or composition, such as adding specific surface coatings, can significantly affect charge-trap characteristics and thereby alter charge-decay rates [35]. These insights corroborate the obtained findings that charge stability and any polarity-based asymmetry are inherently tied to material trap properties, and they highlight that the targeted material modifications can further optimise electret performance.

Charge levels of the electret film

Immediately after charging the PET electret film samples by corona discharge, two parameters were measured: (1) the total charge Q_T on the sample using a Faraday cup, and (2) the maximum surface potential U_{max} at the centre of the charged side A. The results of these measurements are shown in Figure 6.

As it can be seen in Figure 6, there is a clear dependence of both stored charge and surface potential on the applied charging voltage U_e. A higher charging voltage (stronger polarising field) injects more charge into the dielectric, leading to a greater surface potential. Both the maximum surface potential U_{max} and the total charge Q_T typically exhibit an approximately linear increase with the applied corona voltage U_e. However, at +6 kV, a noticeable deviation from the given trend is observed. The underlying cause of this deviation is discussed later in this section. The highest recorded total (i.e., net) charge values are approximately Q_T = +33 nC for U_e = +10 kV and Q_T = −29 nC for U_e = −10 kV.

On the basis of U_{max} measurements, the inception voltage U_i for corona discharge can be calculated. In the conducted experiments, for negative corona U_{i-} is -3.6 kV, whereas for positive corona U_{i+} equals +5.6 kV.

Within the investigated range, the relation between the maximum surface potential U_{max} and the charging voltage U_e (assuming $|U_e| > |U_i|$) can be presented for positive corona discharge as:

$$U_{max} = 1.0 \cdot \left(U_e - U_{i+} \right) \tag{4}$$

and for negative corona discharge as:

$$U_{max} = 0.84 \cdot \left(|U_e| - |U_{i-}| \right) \tag{5}$$

It can be assumed that for the charging voltage of +6 kV, the corona discharge is not very stable. The previously mentioned Q_T deviation from the linear trend (for U_e = +6 kV) is most likely due to only a slight difference between the inception voltage U_i and the charging voltage U_e.

In the next part of the study, a scanning and mapping technique was used in the surface potential measurement. The proposed method enables the measurement of the complete surface charge distribution profile of electrets and provides a potential mapping graph that reflects the exact surface charge distribution and the charge decay trend after corona charging [36, 37].

The results of surface potential distribution measurements along the sample diameter are shown in Figure 7 for different times after the charging process. The obtained results confirm that the potential generally reaches a peak near the centre of the film (i.e., in the area directly under the needle electrode) and decays with time. As shown in Figure 7, over time, the peak potential value decreases, and the distribution broadens significantly. In other words, as the charge decays, the spatial profile becomes flatter and wider. The observed behaviour can be attributed to two mechanisms. First, there is a radial charge diffusion effect, in which the surface charge migrates from areas of higher concentration (usually near the centre of the sample) towards the edge of the sample (with lower charge density), leading to a

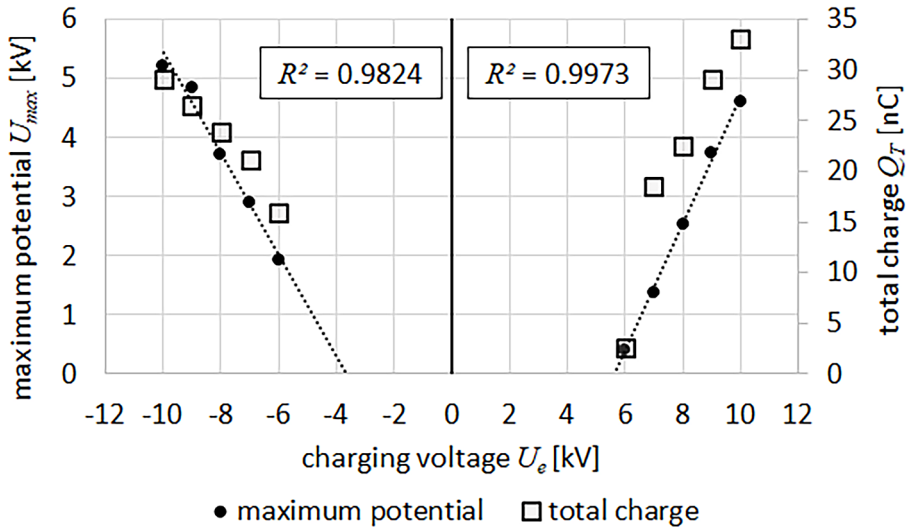

Figure 6. Maximum surface potential U_{max} and total charge Q_T as a function of charging voltage U_e, R^2 values are given for U_{max}

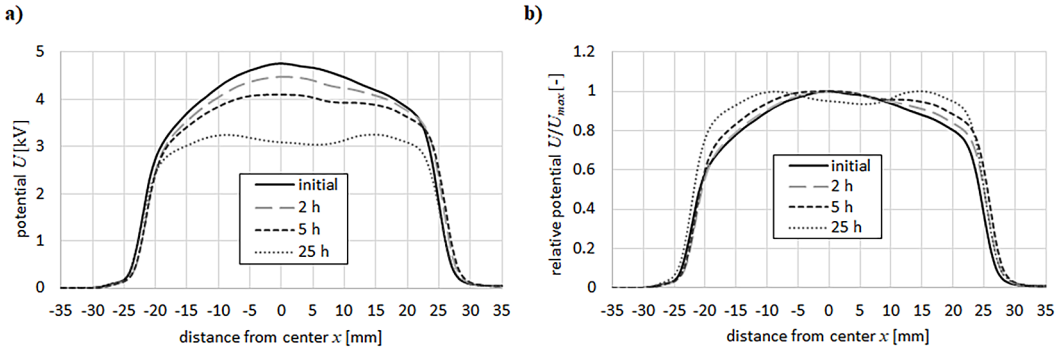

Figure 7. Measured surface potential distribution (U_e = +10 kV): (a) real, and (b) normalised patterns

broader and flatter potential profile. Secondly, the non-uniform rate of charge decay at the surface contributes to the observed shape. Specifically, the potential tends to decay faster in the areas where it was initially higher (i.e., the centre of the sample) and slower where it was lower (i.e., the edges of the sample). This results in a broadening of the charge distribution over time. A similar trend is also observed in [38], where the effect was even more prominent. However, it is worth noting that this study involves a different material (HTV silicone rubber), which can affect the dynamics of charge changes.

It was also observed that the shape of the surface potential distribution profile is strongly dependent on the magnitude of the charging voltage (i.e., supplying the corona electrode). The influence of the charging voltage of the PET film samples on the surface potential distribution is shown in Figure 8. The shape of the surface potential profile was found to depend on the magnitude and polarity of the corona charging voltage. Figure 8 compares normalised potential distributions for different U_e values. In general, higher charging voltages produce a wider charge distribution on the sample. This effect is especially evident for positively charged samples. Notably, the profile obtained at U_e = +6 kV is much narrower than those at higher voltages, which correlates with the lower total charge deposited at 6 kV (see Figure 6). Since +6 kV is very close to the positive inception voltage (U_{i+} = +5.6 kV), operating at this threshold likely led to a more localised charging with limited spread, due to the marginal and unstable corona discharge in that case. Furthermore, under comparable conditions (same $|U_e|$ value, charging time, humidity), negatively charged samples exhibited slightly broader surface potential profiles than positively charged ones. Figure 9 shows an example comparison at U_e = 10 kV: the negative-corona charged film has a marginally wider potential distribution, though apart from this width difference, the overall "bell" shape of the profile is similar for both polarities. Aside from the width, any other systematic difference in profile shape between positive and negative corona charging were not observed.

The surface potential mapping was extended to the entire area of the film on both sides. An example 2D potential map for side A is shown in Figure 10 (for a sample charged at –10 kV).

The distribution is approximately axisymmetric and bell-shaped, with the highest potential at the centre of side A (under the needle during charging).

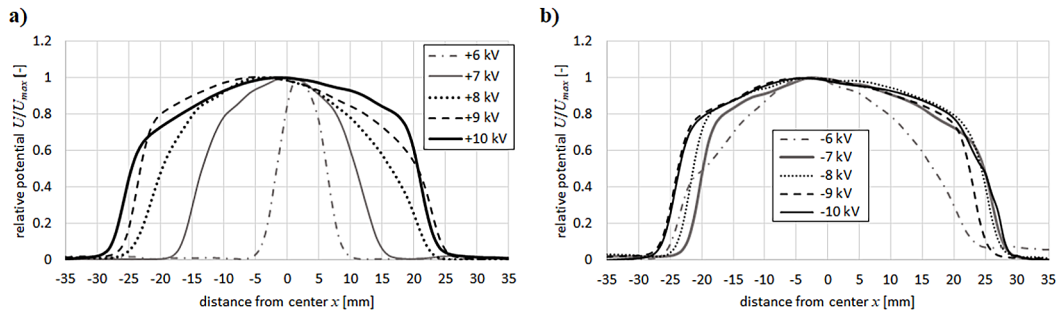

Figure 8. Measured surface potential distribution (normalised) patterns along the sample diameter for: (a) positive, and (b) negative charging voltage

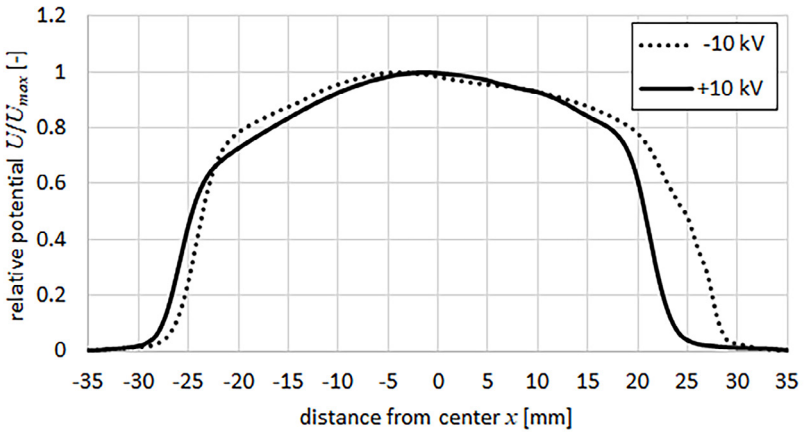

Figure 9. Measured surface potential distribution (normalised) patterns along the sample diameter for both polarities of charging voltage

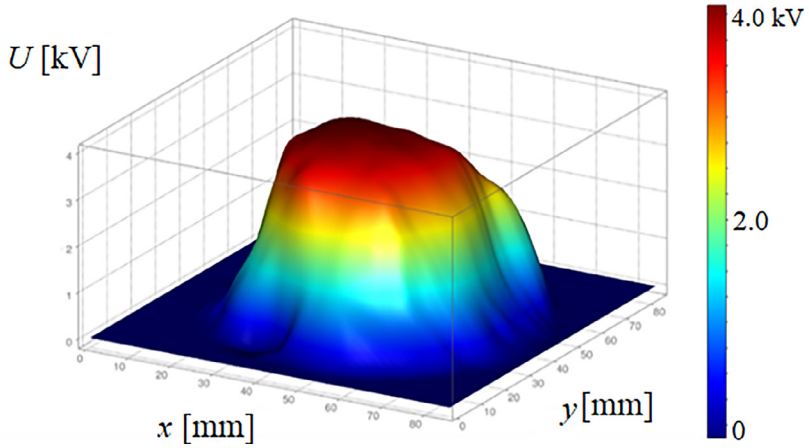

Figure 10. Pattern of the surface potential distribution on the charged side during corona discharge; U_e = -10 kV

Such bell-shaped surface potential profiles are typical for corona-charged dielectric films [38, 39]. They arise from the inherent non-uniformity of the electric field in the point-to-plane corona geometry [38–40]: the electric field (and thus charge deposition rate) is strongest directly beneath the corona point and diminishes radially outward, yielding a peaked charge distribution. The measured potential map on side B had a similar shape, with opposite polarity (since side B acquires a charge of the opposite sign to the polarity of the charging voltage) and slightly lower potential values. However, it is important to note that mapping the full surface is time-consuming. In the conducted measurements, scanning the entire side A took roughly 4600–5600 s, and the scan of side B was performed immediately afterward, finishing at about 8300 s after the initial charge. This means that significant charge decay (estimated 5–20% reduction) could occur for the measurement, especially by the time side B was being scanned. Knowing the decay characteristics from Figure 5, a time-dependent correction was applied to the measured potentials to account for the expected decay during scanning. Essentially, the measured value of each point was adjusted based on the elapsed time and the decay curve (assuming the spatial profile shape does not itself change the decay, aside from the diffusion broadening already discussed). Figure 11 shows the surface potential profiles along the central diameter on both side A and side B after applying this decay correction. The corrected full-area measurements (Figure 11) confirm that side B of the film consistently carries an induced charge of opposite polarity to side A and of nearly the same magnitude. In most cases, the peak surface potential on side B is only slightly lower than on side A. For example, U_{maxA} = 5.18–5.23 kV, whereas U_{maxB} = 5.10–5.14 kV – a difference of

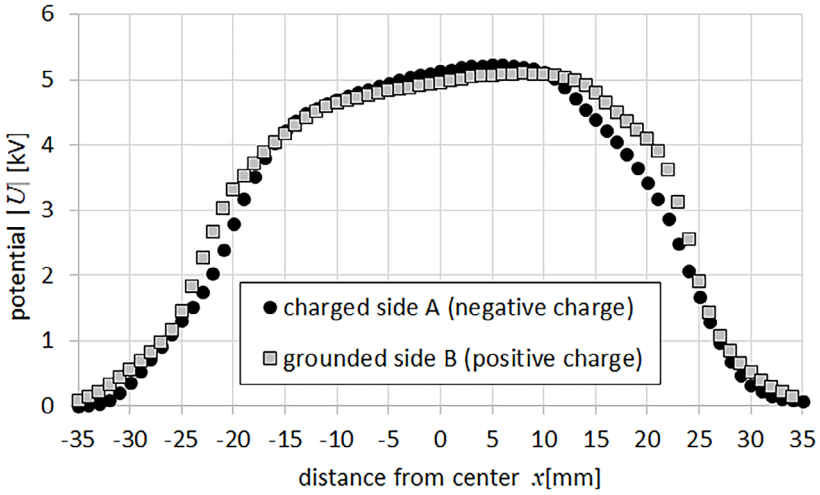

Figure 11. Surface potential distribution along the sample diameter on two sides of the sample; U_e = -10 kV

only about 1-2%, which is within the measurement uncertainty. Thus, aside from the polarity inversion, the charged side and the opposite side have comparable surface potential levels immediately after charging. We also observe that the potential distribution on side B is somewhat broader (more spread out) than on side A. This is likely because side B was scanned later, after the charge had time to undergo the diffusion and non-uniform decay broadening described above. In general, for charging voltages of ±10 kV, the measured potential profiles (on either side) can be fit reasonably well by a sinus-type analytical function. It was found that a function of the form $\cos^{0.8}(A \cdot x)$ (where A is a constant related to the sample geometry and size) provided a good fit (coefficient of determination $R^2 = 0.972$) to the normalised diameter profiles (see Figure 12 for a comparison of measured and fitted curves). As mentioned earlier, the maximum surface potential on side A after charging (at ±10 kV) was about 5.2 kV. Using this value, the surface charge density on the film can be estimated. Assuming a parallel-plate capacitor model for the film on the grounded plate (with known film thickness and dielectric constant), the surface charge density is given by [37]:

$$q_{s\max} = \frac{\varepsilon_0 \varepsilon_r U_{\max}}{d_s} \tag{6}$$

Applying 5.2 kV as U_{max} (and the PET film parameters), a maximum surface charge density on the order of 4.2 mC/m² was obtained. Using the fitted $\cos^{0.8}(A \cdot x)$ charge distribution with this peak value, the total charge on one side of the sample can be estimated by integrating over the area. For side B, this integration yields on the order of a few microcoulombs of charge (approximately 6.17 µC for side B, given the assumed profile). If

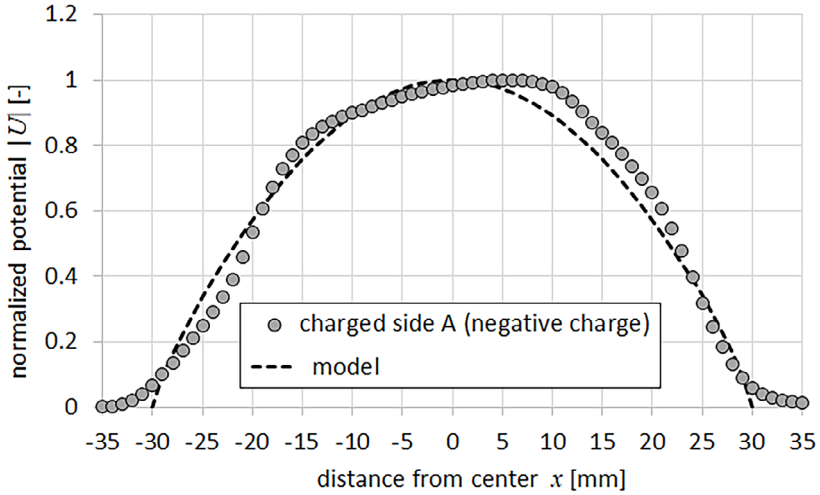

Figure 12. Measured and simulated potential distribution profiles along the sample diameter

side A is assumed to carry a similar distribution but about 0.5% more charge (consistent with its slightly higher U_{max}, then the net charge difference between the two sides would be roughly 30.8 nC. This agrees well with the net charge measured directly by the Faraday cup (which ranged from 29 nC to 33 nC for these samples, see Figure 7). The close agreement suggests that the measured surface potential profiles and assumptions about the charge distribution are consistent. In other words, side B carries nearly the same amount of charge as side A (within about 0.5% less), so the electret charging is almost symmetric between the two surfaces. It was noted, however, that these calculated absolute charge values depend on the assumed profile shape and peak density; thus, they should be taken as indicative estimates.

In conclusion, the measurement results indicate that the material effectively retains charge, with a charge decay time of $t_{95\%} > 950$ s. This suggests that the PET film exhibits good electret properties after corona charging. The surface potential distribution on the film is reproducible and stable under repeated charging conditions, indicating that the corona charging process is consistent and yields similar charge profiles in particular experiments. These results confirm that the selected PET film can store a significant quasi-permanent charge, behaving as a viable electret for subsequent electroadhesion measurements.

Electrostatic force measurements

Measurements of the attractive force F_a between PET charged film and the conductive (grounded) surface were carried out using the system shown in Figure 4. In these experiments, the PET film was first corona charged, then brought near a grounded metal plate while the attractive force was recorded. The authors concentrated on the samples charged at $|U_e| = 7$–10 kV, because in this range the corona discharge is stable and provides consistently shaped surface potential distributions on the film. Representative force-distance characteristics for negative and positive polarity of the corona discharge are presented in Figure 13.

Each curve, presended in Figure 13, corresponds to a different charging voltage U_e. As expected, higher corona voltages (which deposit more charge on the film) generally led to stronger adhesive forces. Indeed, an almost linear correlation was observed between U_e and both the total accumulated charge Q_T on the film and the maximum surface potential U_{max} on the film (see Figure 7). Thus, increasing the corona charging voltage effectively increases the electret charge, which in turn increases the electrostatic attraction force.

Figure 14 illustrates how the attractive force F_a depends on the separation distance d between the charged film and the grounded surface. The data shown correspond to the case that yielded the highest measured force (among our test conditions). In Figure 14a, the full range of film-to-ground distances (from 0.5 mm up to tens of millimeters) is plotted, while Figure 14b provides a magnified view of the force behaviour at short distances (0.5 to 4 mm). It was found that at small gaps, the force drops off with distance in a manner that can be fit by a logarithmic function. A logarithmic trendline $A_F \cdot \ln(d) + B_F$ (where A_F and B_F are scaling parameters), provided an excellent fit to the data in the 0.5–4 mm range ($R^2 > 0.99$).

For an ideal parallel-plate capacitor with infinite electrode area and a fixed charge on the plates, the electrostatic force is theoretically independent of the gap distance (since the field remains uniform) – see Equation 3. However, in the adopted experimental configuration, the PET film electrode is of finite size and not perfectly aligned with the grounded plate, and there are significant

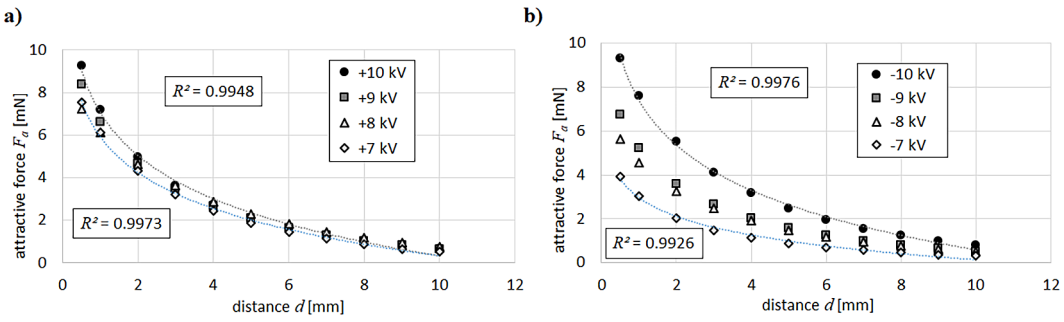

Figure 13. Average attractive force F_a for: a) positively, and b) negatively charged samples ($|U_e| = 7$–10 kV)

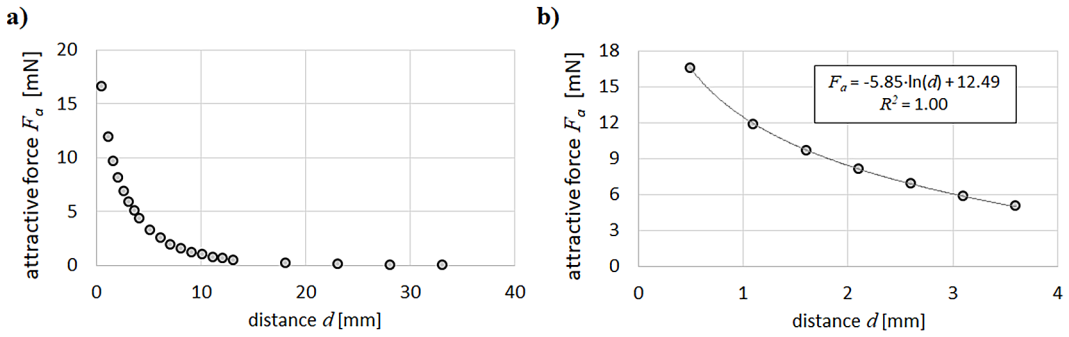

Figure 14. Maximum recorded electrostatic force F_a for: (a) the full range of electret film-to-ground surface distance, and (b) short distances (up to 4 mm)

edge (fringing) effects. These geometric limitations cause substantial deviations from the ideal parallel-plate behaviour. As a result, the measured electrostatic adhesion force in the studied system is strongly dependent on the film–surface separation d. In particular, the force of attraction is highest when the film is very close to the grounded surface, and it decreases rapidly as the gap increases.

In particular, the force of attraction is highest when the film is very close to the grounded surface, and it decreases rapidly as the gap increases. The largest recorded force was F_a = 16.6 mN at the smallest tested distance d = 0.5 mm. Over the short-range region (d = 0.5–4 mm), F_a decays sharply (nearly logarithmically, as noted above) with increasing distance. At larger separations (more than ~25 mm), F_a falls to below about 0.1 mN, essentially reaching negligible levels for practical purposes. This distance-dependent trend is in qualitative agreement with expectations for a finite-sized charge patch: the Coulombic attraction weakens substantially when the charged film is moved farther from the grounded target, due to field spreading and edge effects that reduce the effective field coupling. From the force–distance data, an approximate "adhesion pressure" corresponding to the electrostatic attraction, defined as the force per unit area over the charged film's surface can also be computed. In the adopted setup (with a circular film of diameter 47 mm, see Figure 3), the peak adhesion pressure just before contact (at d = 0.5 mm and at the highest charge) was about 9.6 Pa. This value is low in an absolute sense (reflecting the modest charge levels on the electret), but it is achieved with zero continuous power input since the film is charged beforehand and acts as a passive adhesive. Such adhesion pressures might be sufficient for certain applications where reversible and residue-free attachment is needed, especially considering that they can be modulated by adjusting the charge on the film and the gap.

Figure 15 shows the average electrostatic attractive force F_a on the maximum surface potential U_{max} for two fixed gap distances (0.5 mm and 3 mm), under both positive and negative charging.

The general trend is that a higher surface potential (and thus a higher surface charge) yields a greater attractive force, which is expected. More interestingly, one can see that increasing the gap from 0.5 mm to 3 mm consistently leads to a reduction in F_a for a given U_{max}. This reduction occurs for both positively and negatively charged films and across all surface potential values tested. The drop in force due to the increased distance is roughly uniform in percentage terms, although it becomes most pronounced at the highest surface potentials (where moving from 0.5 mm to 3 mm reduced the force by about a factor of 2.5).

Comparing the studied PET film system to an idealised scenario helps to contextualise the results. If the charged film and grounded surface behaved like two parallel plates without fringing and without any free charge dissipation, one would expect the force to scale with the square of the charge or surface potential ($F_a \propto Q^2$ or $F_a \propto U^2$). In the conducted experiments, the relationship between force and charge is more complex due to the non-uniform charge distribution on the film and its finite size. A simple quadratic scaling of F_a with U_{max} or Q_T over the entire range was not observed, which is unsurprising given the earlier noted geometry effects. Moreover, a subtle difference between positive and negative corona-charged samples was found: the increase of F_a with charging voltage (and thus with stored charge) was somewhat weaker for positively charged films than for negatively charged ones. In other words, at equivalent high $|U_e|$, the negative-charged films tended

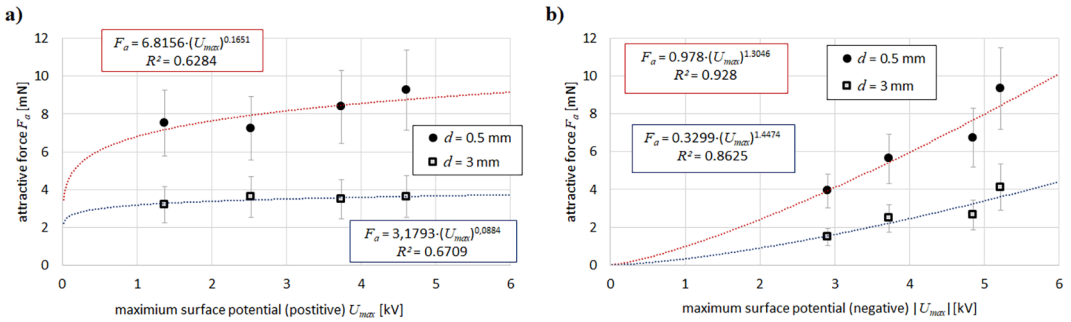

Figure 15. Average electrostatic attractive force as a function of maximum surface potential for two sample-conductive surface (grounded) distances *d* equal to 0.5 mm and 3 mm: (a) positive polarity, and (b) negative polarity of charging voltage

to provide slightly higher forces than the positive-charged films, relative to their surface potentials. This discrepancy may be related to differences in space charge distribution in the air gap or in how the charge of each polarity decays or redistributes on the film over time, or to the influence of fringing fields resulting from the electrode configuration. It suggests that the polarity of charging could influence not just charge retention (as discussed earlier) but also the effective adhesion force, possibly through secondary effects like air ionisation or different trap depths for positive vs. negative charge. However, a full explanation of the cause of this polarity-dependent force behaviour is beyond the scope of the present work and requires further in-depth study.

CONCLUSIONS

Conventional, active EA implementations require a continuous high-voltage power supply to maintain the adhesive force, which adds complexity and limits their practicality in some applications. To overcome this limitation, recent research has explored passive electroadhesion techniques that do not require continuous power input. In passive EA, the adhesive force is provided by charges stored in the materials themselves (for example, using charged dielectric layers), eliminating the need for an active voltage source during operation. Polyethylene terephthalate (PET) films charged by DC corona exhibited strong electret behaviour, with the polarity and magnitude of charging significantly influencing the surface charge characteristics. The PET electrets long charge storage times ($t_{95\%}$ > 980 s). Immediately after charging, the surface potential on the PET film had a bell-shaped lateral distribution peaking beneath the corona electrode, reflecting the non-uniform field geometry of the point-to-plate discharge. Both the directly charged front side and the opposite grounded side of the film acquired similar charge patterns of opposite polarity; their surface potential profiles were approximately symmetrical, with the back side showing a slightly lower peak value. Increasing the corona voltage led to higher deposited charge and higher peak surface potential (approximately linear with voltage up to 10 kV). The polarity of the corona had a significant effect on charge distribution: negative polarity produced a more uniform surface potential profile with a higher maximum potential than positive charging at the same voltage, although the total deposited charge was lower for negative corona. Over time, the initially localised charge distributions broadened as the charges diffused and decayed across the surface, consistent with diffusion-driven charge migration and the cross-over effect (where regions of higher initial charge density decay faster). These results confirm that PET films can be effectively charged as electrets, with controllable charge profiles and retention characteristics governed by the charging conditions.

The charged PET films were also shown to generate measurable electrostatic adhesion forces to a grounded conductive surface, and these forces depended strongly on the surface charge (surface potential) and the separation distance. Higher surface potential on the film (i.e., greater stored charge) yielded a stronger attractive force, while increasing the film-to-surface distance led to a rapid decline in the adhesion force. For instance, at a small gap of 0.5 mm the PET electret exhibited a peak attractive force on the order of 10^{-2} N (up to approximately 16.6 mN for the highest charge densities achieved), whereas enlarging the gap to 3 mm reduced the force by roughly a factor of 2.5,

and at distances beyond about 25 mm the force fell below 0.1 mN – essentially negligible for practical purposes. These measurements demonstrate that a corona-charged PET film can act as a reusable passive electroadhesive: it provides a repeatable adhesive force to a grounded object without requiring continuous power input after charging. In practical terms, the PET electret achieved an adhesive pressure of only a few pascals (maximum ~9.6 Pa in the considered setup), indicating that while the adhesion is reliable, its strength is low and best suited for light loads or temporary attachment. The performance is inherently limited by the non-uniform charge distribution and finite size of the film – factors that cause deviations from idealised parallel-plate behaviour and constrain the effective range of the electrostatic force. Additionally, the marked difference in charge decay between positive and negative charging means that the longevity of the adhesive effect can vary with the chosen charging polarity (with positively charged films maintaining their surface charge, and thus adhesive capability, much longer than negatively charged ones under similar conditions).

Overall, the findings of this study verify that PET films can serve as stable electret-based adhesive surfaces, and they provide quantitative insight into how charging parameters control both the stored charge profile and the resulting adhesion force. These results not only meet the stated objectives of characterising the electret behaviour and adhesion performance of PET under different charging conditions but also offer a basis for the development of low-power electroadhesive applications. By highlighting the relationships between charge input, retention, and adhesive output, the work helps to identify both the potential and the limitations of PET electret films in practical electroadhesion technologies.

REFERENCES

1. Chang J.S., Kelly A.J., Crowley J.M. Handbook of Electrostatic Processes. CRC Press; 1995.
2. Lüttgens G., Lüttgens S., Schubert W. Static Electricity: Understanding, Controlling, Applying. John Wiley & Sons; 2017.
3. Zahn M. Electromagnetic field theory: A problem solving approach. Krieger Publishing Company; 2003.
4. Inculet II. Electrostatics in Industry. J. Electrostat. 1978; 4(2): 175–92. https://doi.org/10.1016/0304-3886(78)90071-2
5. Du C., Huang W., Lei Y. The application and prospects of 3D printable microgel in biomedical science and engineering. Int. J. Bioprint. 2023; 9(5): 753. https://doi.org/10.18063/ijb.753
6. Chai J., Zhang K., Xue Y., Liu W., Chen T., Lu Y., Zhao G. Review of MEMS based Fourier transform spectrometers. Micromachines. 2020; 11(2): 214. https://doi.org/10.3390/mi11020214
7. Breshears M., Giridharagopal R., Pothoof J., Ginger D. A robust neural network for extracting dynamics from electrostatic force microscopy data. J. Chem. Inf. Model. 2022; 62(18): 4342–50. https://doi.org/10.1021/acs.jcim.2c00738
8. Xu G., Li C., Chen C., Fu J., Hou T., Zi Y. Dynamics of triboelectric nanogenerators: a review. Int. J. Mech. Syst. Dyn. 2022; 2(4): 311–24. https://doi.org/10.1002/msd2.12058
9. England S., Robert D. Electrostatic pollination by butterflies and moths. J. R. Soc. Interface. 2024; 21: 20240156. https://doi.org/10.1098/rsif.2024.0156
10. Gholami S., Aarabi M., Grabowski S. Coexistence of intra- and intermolecular hydrogen bonds: salicylic acid and salicylamide and their thiol counterparts. J Phys Chem A. 2021; 125(7): 1526–39. https://doi.org/10.1021/acs.jpca.0c11183
11. Guo J., Leng J., Rossiter J. Electroadhesion technologies for robotics: A comprehensive review. IEEE Trans. Robot. 2020; 36(2): 313–27. https://doi.org/10.1109/TRO.2019.2956869
12. Guo J., Leng J., Rossiter J. Enhancing humans and machines with ubiquitous electroadhesives. Matter. 2022; 5(2): 368–71. https://doi.org/10.1016/j.matt.2022.01.013
13. Monkman G. Workpiece retention during machine processing. Assembly Automation. 2001; 21(1): 61–7. https://doi.org/10.1108/01445150110381754
14. Cao J., Qin L., Liu J., Ren Q., Foo C.C., Wang H., et al. Untethered soft robot capable of stable locomotion using soft electrostatic actuators. Extreme Mech. Lett. 2018; 21: 9–16. https://doi.org/10.1016/j.eml.2018.02.004
15. Wang H., Yamamoto A., Higuchi T. A crawler climbing robot integrating electroadhesion and electrostatic actuation. Int. J. Adv. Robot. Syst. 2014; 11: 1–11. https://doi.org/10.5772/5911
16. Guo J., Xiang C., Rossiter J. Electrically controllable connection and power transfer by electroadhesion. Smart Mater. Struct. 2019; 28(10): 105012. https://doi.org/10.1088/1361-665X/ab383b
17. Graule M.A., Chirarattananon P., Fuller S.B., Jafferis N.T., Ma K.Y., Spenko M., et al. Perching and takeoff of a robotic insect on overhangs using switchable electrostatic adhesion. Science. 2016; 352(6288): 978–82. https://doi.org/10.1126/science.aaf1092

18. Ruffatto D., Glick P.E., Tolley M.T., Parness A. Long-duration surface anchoring with a hybrid electrostatic and gecko-inspired adhesive. IEEE Robot. Autom. Lett. 2018; 3(4): 4201–8. https://doi.org/10.1109/LRA.2018.2856366
19. Guo J., Xiang C., Rossiter J. A soft and shape-adaptive electroadhesive composite gripper with proprioceptive and exteroceptive capabilities. Mater. Des. 2018; 156: 586–7. https://doi.org/10.1016/j.matdes.2018.07.027
20. Guo J., Bamber T., Zhao Y., Chamberlain M., Justham L., Jackson M. Toward adaptive and intelligent electroadhesives for robotic material handling. IEEE Robot. Autom. Lett. 2017; 2(2): 538–45. https://doi.org/10.1109/LRA.2016.2646258
21. Zhang S., Shao S., Yang X., Chen P., Ji H., Liu K., et al. An enhanced flexoelectric dielectric elastomer actuator with stretchable electret. Smart Mater Struct. 2021; 30: 125004. https://doi.org/10.1088/1361-665X/ac2de1
22. Tian Z., Li Y., Li Y., Han W., Ji H., Zhang S., et al. A mechanical manipulated electromechanical coupling design with stretchable electret film: mechanical sensing, energy harvesting, and actuation. Smart Mater. Struct. 2024; 33: 065031. https://doi.org/10.1088/1361-665X/ad4938
23. Huang S., Li Y., Zhang S., Zhao H., Song S., Zhai C., et al. Electroadhesion-driven friction enhancement using electret films. Extreme Mech. Lett. 2024; 73: 102270. https://doi.org/10.1016/j.eml.2024.102270
24. Rybarczyk J.B., Górski F., Kuczko W., Wichniarek R., Siwiec S., Vitkovic N. et al. Mechanical properties of carbon fiber reinforced materials for 3D printing of ankle foot orthoses. Advances in Science and Technology Research Journal. 2024; 18(4): 191–215. https://doi.org/10.12913/22998624/188819
25. Ferdynus M., Rogala M. Numerical crush analysis of thin-walled aluminium columns with square cross-section and a partial foam filling. Advances in Science and Technology Research Journal. 2019; 13(3): 144–51. https://doi.org/10.12913/22998624/110611
26. Mendivil-Escalante J.M., Almaral-Sánchez J.L., Gómez-Soberón J.M., Arredondo-Rea S.P., Corral-Higuera R., Castro-Beltrán A. et al. New Concrete Additive By Chemical Recycling Of Pet. Advances in Science and Technology Research Journal. 2014; 8(23): 1–5. https://doi.org/10.12913/22998624.1120307
27. Molinié P. How fast does a static charge decay? An updated review on a classical problem. J. Electrostat. 2024; 124: 03930. https://doi.org/10.1016/j.elstat.2024.103930
28. Rychkov D., Rychkov A., Efimov N., Malygin A., Gerhard R. Higher stabilities of positive and negative charge on FEP electrets treated with titanium-tetrachloride vapor. Appl. Phys. Lett. 2013; 102: 283–7. https://doi.org/10.1007/s00339-013-7821-1
29. Herous L., Remadnia M., Kachi M., Nemamcha M. Decay of Electrical Charges on Polyethylene Terephthalate Surface. J. Eng. Sci. Technol. Rev. 2009; 2(1): 87–90. https://doi.org/10.25103/jestr.021.17
30. Zhang H., Liu N., Zeng Q., Liu J., Zhang X., Ge M., et al. Design of polypropylene electret melt blown nonwovens with superior filtration efficiency stability through thermally stimulated charging. Polymers. 2020; 12(10): 2341. https://doi.org/10.3390/polym12102341
31. Zhang J., Chen G., Gao X. Change of electrostatic field polarity in the melt-blown polypropylene electret fabrics with corona charging. J. Phys. D Appl. Phys. 2023; 56(38): 385308. https://doi.org/10.1088/1361-6463/acdfdb
32. Hu L., Li X., Guo X., Xu M., Shi Y., Herve N.B., et al. Electret modulation strategy to enhance the photosensitivity performance of two-dimensional molybdenum sulfide. ACS Appl. Mater. Interfaces. 2023; 15(51): 59704–13. https://doi.org/10.1021/acsami.3c14836
33. Wang A., Zhang X., Gao L., Zhang T., Xu H., Bi Y. A review of filtration performance of protective masks. Int J. Environ. Res. Public Health. 2023; 20(3): 2346. https://doi.org/10.3390/ijerph20032346
34. Dai N., Guan X., Lu C., Zhang K., Xu S., Lei I., et al. A flexible self-powered noncontact sensor with an ultrawide sensing range for human-machine interactions in harsh environments. ACS Nano. 2023; 17(24): 24814–25. https://doi.org/10.1021/acsnano.3c05507
35. Luo A., Xu Y., Zhang Y., Zhang M., Zhang X., Lu Y., Wang F. Spray-coated electret materials with enhanced stability in a harsh environment for an MEMS energy harvesting device. Microsyst. Nanoeng. 2021; 7(1): 1–9. https://doi.org/10.1038/s41378-021-00239-0
36. Li T., Gao F., Shang H. Surface charge decay patterns of insulating polymers based on potential-mapping method. Emerg. Mater. Res. 2019; 8(4): 634–7. https://doi.org/10.1680/jemmr.17.00059
37. Kacprzyk R. Measurement methods in electrostatics (in Polish). Wrocław: Oficyna Wydawnicza Politechniki Wrocławskiej; 2013.
38. Kacprzyk R., Pelesz A. Charge decay on composite insulators (in Polish). Przegl. Elektrotechn. 2014; 90(10): 16–8. https://doi.org/10.12915/pe.2014.10.04
39. Kumara S,. Hoque I.R., Alam S., Serdyuk Y.V., Gubanski S.M. Surface charges on cylindrical polymeric insulators. IEEE Trans. Dielectr. Electr. Insul. 2012; 19(3): 1076–83. https://doi.org/10.1109/TDEI.2012.6215115
40. Giacometti J.A., Oliveira O.N. Corona charging of polymers. IEEE Trans. Electr. Insul. 1992; 27(5): 924–43. https://doi.org/10.1109/14.256470